

Resonant magneto-optic Kerr effect in the magnetic topological insulator $\text{Cr:}(\text{Sb}_x, \text{Bi}_{1-x})_2\text{Te}_3$

Shreyas Patankar,^{1,2} J. P. Hinton,^{1,2} Joel Griesmar,^{1,2} J. Orenstein,^{1,2,*} J. S. Dodge,³ Xufeng Kou,⁴ Lei Pan,⁴ Kang L. Wang,⁴ A. J. Bestwick,^{5,6} E. J. Fox,^{5,6} D. Goldhaber-Gordon,^{5,6} Jing Wang,^{5,6} and Shou-Cheng Zhang^{5,6}

¹*Department of Physics, University of California, Berkeley CA 94720, USA*

²*Materials Science Division, Lawrence Berkeley National Laboratory, Berkeley CA 94720, USA*

³*Department of Physics, Simon Fraser University, Burnaby, British Columbia, VST 1Z1, Canada*

⁴*Department of Electrical Engineering, University of California, Los Angeles, CA 90095, USA*

⁵*Department of Physics, Stanford University, Stanford, CA 94305, USA*

⁶*Stanford Institute for Materials and Energy Sciences, SLAC National Accelerator Laboratory, 2575 Sand Hill Road, Menlo Park, California 94025, USA*

(Dated: July 14, 2022)

We report measurements of the complex Kerr rotation angle, Θ_K , in thin films of the magnetically doped topological insulator $(\text{Cr}_{0.12}\text{Bi}_{0.26}\text{Sb}_{0.62})_2\text{Te}_3$ as a function of photon energy in the range $0.8 \text{ eV} < \hbar\omega < 3.0 \text{ eV}$. We observe a peak in the real part of $\Theta_K(\omega)$ and corresponding zero crossing in the imaginary part, that we attribute to resonant interaction with a spin-orbit avoided crossing and Dirac band located $\approx 1.7 \text{ eV}$ above the chemical potential. The resonant enhancement allows measurement of the temperature and magnetic field dependence of Θ_K in the ultrathin film limit, $d \geq 2$ quintuple layers. We find a sharp transition to remnant $\Theta_K = 0$ for $d < 8$ QL, consistent with theories of the dependence of impurity spin interactions on film thickness and their location relative to topological insulator surfaces.

PACS numbers: 73.20.-r, 78.20.Ls, 78.66.Li

Three dimensional (3D) topological insulators (TIs) [1, 2] are realizations of quantum matter that manifest protected surface states with Dirac-like energy dispersion. The novel features of TI electrodynamics are expressed in the “axion” term in the Lagrangian, $L = (\theta/2\pi)(\alpha/2\pi)\mathbf{E} \cdot \mathbf{B}$, where θ has value the π (modulo 2π) in the case of a strong 3D TI [3, 4], and $\alpha = e^2/\hbar c$ is the fine structure constant. When θ is uniform in space the axion term has no observable effects because $\mathbf{E} \cdot \mathbf{B}$ is a total space-time derivative and does not modify the equations of motion. However, observable consequences occur at the interface between topologically trivial and non-trivial media, where a 2D Dirac metal is found. If the Dirac spectrum is gapped by a time-reversal symmetry (TRS) breaking perturbation, half-integral Hall conductivity, $\sigma_H = \pm e^2/2h$, is expected when the chemical potential lies in the gap [3].

In practice the half-integral quantum Hall effect (or equivalently, the quantized magnetoelectric effect) is difficult to observe because of parallel current paths that exist either through the bulk or side facets of the crystal that remain gapless despite the breaking of TRS. As a result, epitaxially-grown thin films are playing an increasing role in exhibiting the electromagnetic phenomena associated with 3D TI [5]. Particularly interesting physics arises in the transition from 3D to 2D, as realized for example in films in which the thickness can be tuned with atomic precision. At finite thickness, the top and bottom surfaces are coupled, resulting in two degenerate copies of a massive Dirac spectrum with an energy gap, Δ_t , equal to twice the hopping matrix element, t . The development

of this gap has been observed directly by *in situ* angle-resolved photo-emission spectroscopy (ARPES) [6]. A striking prediction is that, in certain ranges of film thickness, breaking of TRS by ferromagnetic (FM) order will give rise to a quantum anomalous Hall effect (QAHE), that is, integer quantization in the absence of an applied magnetic field [7]. Several recent reports have confirmed integer quantization with increasing accuracy [8–10], although under stringent conditions of temperature, chemical doping, and thickness. For example, quantization in TIs doped with the magnetic impurity Cr is observed only for temperatures in the milli-Kelvin range, despite the fact that spontaneous TRS breaking appears at 15–20K.

To better understand the fragility of the QAHE in magnetic-impurity doped epitaxial films, it is important to probe the strength of the TRS breaking field Δ_z , as a function of film thickness d , temperature T , and magnetic field B . In this work we measure the polarization rotation of light on reflection (Kerr effect), which vanishes in the presence of TRS and is proportional $\Delta_z(d, T, B)$ when TRS is broken. We report measurements of the real and imaginary parts of the Kerr angle Θ_K , from near-IR through visible wavelengths, that is photon energies in the range $0.8 \text{ eV} < \hbar\omega < 3.0 \text{ eV}$. Although, in principle, detecting $\Theta_K(\omega)$ on the energy scale of Δ_z ($\approx 10\text{-}100 \text{ meV}$) might be preferable in terms of direct contact with theoretical predictions [11–14], in practice the present limits on sensitivity in this spectral range make this approach difficult. The magnitude of the Kerr angle predicted theoretically is $\sim \alpha/(\epsilon - 1) \sim 1 \text{ mrad}$, where ϵ

is the bulk (or substrate in the case of an ultrathin film) dielectric constant. Thus, for Θ_K to be an effective probe of Δ_z , particularly the manner in which it vanishes in the limit that $d, T, B \rightarrow 0$, requires ~ 10 - $100 \mu\text{rad}$ sensitivity, which is difficult to achieve in the frequency regime of 2-20 THz.

The Kerr spectra reported here were measured with a W-filament light source and grating monochromator. Phase sensitive detection at the second and third harmonic of a photo-elastic modulator [15, 16] enabled detection with $10 \mu\text{rad}$ resolution, as well as precise discrimination between the real and imaginary parts of the Kerr effect [17]. The samples used for this study were thin films of $(\text{Cr}_{0.12}\text{Bi}_{0.26}\text{Sb}_{0.62})_2\text{Te}_3$ prepared using molecular-beam epitaxy on semi-insulating GaAs (111) substrates. We observed a resonance in the spectrum of the Kerr angle, $\Theta_K(\omega)$, characterized by a peak in the real part and a zero crossing in the imaginary part, both occurring at approximately 1.7 eV. Two-photon ARPES measurements [18] suggest that the resonance is associated with transitions from states near the Fermi energy, ε_F , to states near a spin-orbit avoided band-crossing situated at the Γ point at 1.5-1.8 eV above ε_F . Band-structure calculations predict [19, 20], and two-photon ARPES confirm [18], that there is a second Dirac band (DB2) associated with this avoided crossing that is analogous to the Dirac band (DB1) whose node is near the Fermi energy.

Fig. 1a shows the real, θ_K , and imaginary, ϵ_K , parts of Θ_K in the spectral range from 1.1-2.9 eV for a 20 quintuple-layer (QL) sample measured at $T = 6\text{K}$. As discussed above, the peak energy of 1.7 eV suggests that the Kerr rotation in this frequency range is enhanced by transitions from states near the chemical potential to states near DB2. In the following we describe the extraction of the complex dielectric tensor, $\epsilon_{ij}(\omega)$ from the measured $\Theta(\omega)$ spectra.

Because the optical penetration depth is less than 10 QL over most of the spectral range of our measurement, we model the 20 QL sample as a semi-infinite medium and assume that $\epsilon_{ij}(\omega)$ is uniform throughout the film. In this case,

$$\epsilon_{xy}(\omega) = \frac{\tilde{n}(\tilde{n}^2 - 1)}{2} \Theta_K(\omega), \quad (1)$$

where $\tilde{n}^2(\omega) \equiv \epsilon_{xx}(\omega)$. In the analysis we assume that $\epsilon_{xy} \ll \epsilon_{xx}$ and use the diagonal component of the dielectric function as reported in Ref. [21].

Fig. 1b shows the real and imaginary parts of $\epsilon_{xy}(\omega)$ obtained by analysis of $\Theta_K(\omega)$. There is a striking similarity in both the amplitude and frequency dependence of $\epsilon_{xy}(\omega)$ in $(\text{Cr}_{0.12}\text{Bi}_{0.26}\text{Sb}_{0.62})_2\text{Te}_3$ (Cr:BiSbTe) with spectra that have been obtained from the magnetically doped 3D semiconductor Mn:GaAs [22, 23]. This correspondence suggests that the response in thick films of Cr:BiSbTe is a manifestation of bulk states, rather than

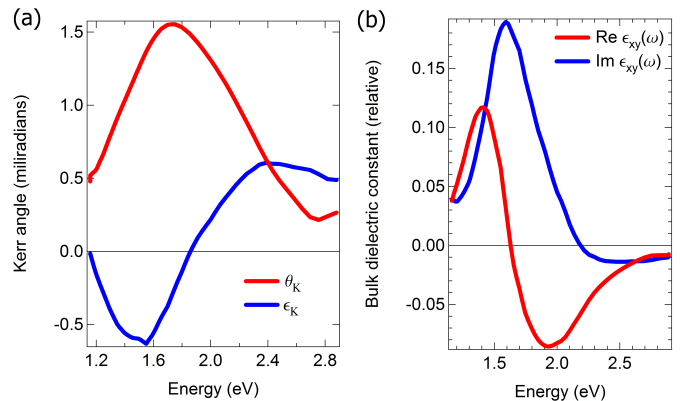


FIG. 1. Kerr effect in a 20 QL thick sample of $(\text{Cr}_{0.12}\text{Bi}_{0.26}\text{Sb}_{0.62})_2\text{Te}_3$. (a) Real θ_K and imaginary ϵ_K parts of the Kerr spectrum measured at 6K with magnetic field of 100mT applied perpendicular to the film plane, (b) off-diagonal component of the dielectric function, $\epsilon_{xy}(\omega)$, as determined by analysis of the Kerr spectra shown in panel (a).

an anomalous response coming specifically from the surface.

Our combined optical and transport studies on samples grown using the same protocol support this idea. The samples in the present study are ungated, so their Fermi level is determined by film stoichiometry. This is not perfectly controlled during growth, and can further change with exposure to air, yielding a range of carrier concentrations for the different samples from -8×10^{12} (i.e., hole doped) to $9 \times 10^{12} \text{cm}^{-2}$ (electron doped), as determined from Hall measurements at temperatures above the magnetic transition [17]. In a subset of the samples studied the anomalous Hall resistance R_{AHE} , at dilution refrigerator temperatures approaches the quantized value $h/e^2 \approx 25.8 \text{k}\Omega$ [9, 10], while other samples grown under nominally the same conditions display R_{AHE} in the range 2 to 17 k Ω . Despite these variations in R_{AHE} , we find that the trends in $\Theta_K(d, T, B)$ are robust. This suggests that the Kerr effect in the near-IR originates from transitions between bulk states, in which case the reproducibility of Θ_K requires only that the chemical potential lie in the bulk gap, which is a much less stringent condition than required for observation of the QAHE.

The appearance of a peak in $\epsilon_{1xy}(\omega) \equiv \text{Re}[\epsilon_{xy}(\omega)]$ and dispersive lineshape of $\epsilon_{2xy}(\omega) \equiv \text{Im}[\epsilon_{xy}(\omega)]$, which is reversed from the usual behavior of $\epsilon_{xx}(\omega)$ in the neighborhood of a resonance, is also consistent with a transition between spin-split bulk valence and conduction bands. The difference in energy between up and down spin induces a shift in the peak of the interband absorption as measured by left and right circularly polarized light. Thus the spectrum of $\epsilon_{2+}(\omega) - \epsilon_{2-}(\omega)$ (where $\epsilon_{2\pm}$ are the imaginary parts of the dielectric function in the circular polarized basis) will resemble the derivative of an absorption peak. Transforming back to the Cartesian ba-

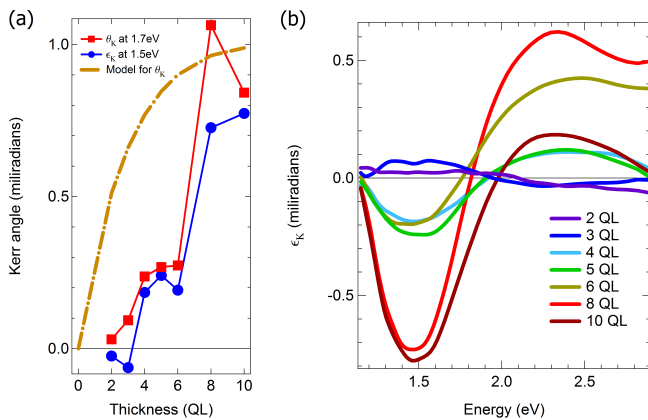


FIG. 2. Thickness dependence of Kerr spectra. (a) Amplitudes of θ_K and ϵ_K at their respective peaks of 1.7eV and 1.5eV as a function of sample thickness at 6K and 100mT. Plotted for comparison (dashed-dot line) is $\theta_K(d)$ calculated under the assumption of d -independent $\epsilon_{xy}(\omega)$, (b) imaginary part of $\Theta_K(\omega)$ for various thicknesses in the range from 2 to 10 QL.

sis, where $\epsilon_{xy}(\omega) = [\epsilon_+(\omega) - \epsilon_-(\omega)]/2i$, shows that spin split bands generically manifest a derivative lineshape for ϵ_{1xy} , as is seen in Fig. 1b.

As mentioned above, we can use the sensitivity of the resonantly enhanced Kerr effect to explore the evolution of the Kerr rotation as a function of film thickness, d , down to the ultrathin limit. Fig. 2a shows the real and imaginary parts of Θ_K at $T = 6$ K as a function of d , with fixed Cr concentration, sampled at their peak photon energies of 1.7 and 1.5 eV, respectively. Fig. 2b shows the imaginary part of $\Theta_K(\omega)$ for the same set of samples, demonstrating that the frequency dependence of the Kerr resonance remains the same even as its amplitude is significantly reduced with decreasing d .

The dependence on thickness is highly structured, with steep changes in amplitude taking place just below 8 and 4 QL and relatively small changes in between these thicknesses. These features can be contrasted with the thickness dependence that would obtain if $\epsilon_{xy}(\omega)$ was independent of sample thickness. To make this comparison, we fitted $\epsilon_{xy}(\omega)$ as measured from the 20 QL film using a Lorentzian function, and then input this fit into the formula for the reflection tensor of a thin film on a dielectric substrate [12]. The result of this simulation is shown as a dashed-dot line in Fig. 2a. Not surprisingly, the assumption of thickness independent $\epsilon_{xy}(\omega)$ predicts that the Kerr rotation decreases smoothly to zero once d becomes smaller than the optical penetration depth. Thus the sharp features in the observed thickness dependence can be attributed to structure in $\epsilon_{xy}(\omega)$ vs. d , and ultimately to structure in $\Delta_z(d)$.

Further evidence for structure in $\Delta_z(d)$ emerges from the T dependence of the Kerr rotation. Fig. 3a shows the $\theta_K(T)$ of a 20 QL film, measured at a photon energy of

1.96 eV. $\Theta_K(T)$ was measured with two different protocols for application of a B field, which yielded markedly different results. In both types of experiment the sample was cooled to 6K with $B \approx 100$ mT applied in the direction normal to the film surface. The data shown in red were recorded after switching the field to zero at 6K and subsequently warming. $\theta_K(T)$ measured under these conditions is therefore related to the remnant magnetization, which extrapolates to zero at ~ 20 K, which we define as the remnant temperature, T_r . The data shown in blue were recorded after again cooling in 100 mT, but with the field left on during the warming cycle. The different results for the two measurement procedures are quite striking and not characteristic of a conventional ferromagnet. Not only is $\theta_K(T)$ in field much larger, but it persists to much higher temperature, ~ 50 K. Thus there is a broad temperature regime, from $\approx 20 - 50$ K, in which the magnetization in zero-field is absent, but the magnetic susceptibility is greatly enhanced relative to the normal state. This anomalous regime likely indicates locally ordered regions whose tendency to align in zero field is frustrated by competing interactions, but will align under the influence of very small applied fields [17].

In Fig. 3b we illustrate the thickness dependence of the remnant magnetization by plotting both T_r and the remnant value of $\Theta_K(6K)$ vs. d . The structured dependence on d is even more clear in the remnant properties than those measured in 100 mT magnetic field. For example, $\Theta_K(6K)$ suddenly becomes too small to measure for sample thicknesses less than 8 QL. We note that samples such as these may exhibit remnant magnetization when

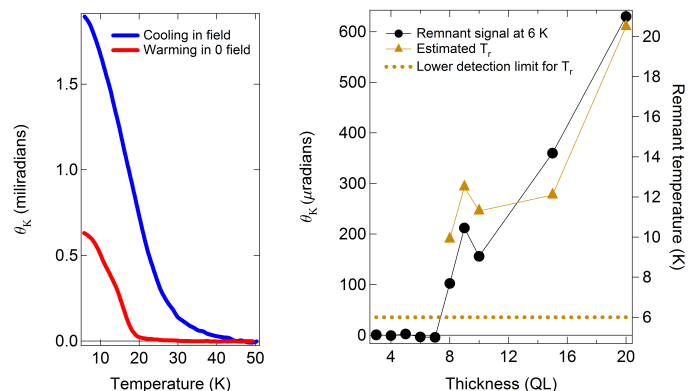


FIG. 3. (a) Real part of the Kerr rotation, θ_K at photon energy 1.96 eV as a function of temperature for a 20 QL film. The larger amplitude curve was measured upon cooling in a 100 mT magnetic field and warming with the field left on, the smaller amplitude curve was recorded on warming with field turned off at 6K, and is a measure of the remnant magnetization, (b) Remnant magnetization as a function of film thickness. Remnant $\Theta_K(6K)$ shown as solid circles (left axis), triangles (right axis) show the temperature T_r above which the remnant signal vanishes. Dashed line indicates our experimental upper bound on T_r .

cooled below 6 K, for example into the miliKelvin range where the QAHE has been observed. Below we comment on possible origins for such structure in $\Delta_z(d)$.

Evidence for a crossover to a regime of strong coupling between top and bottom surface states with decreasing film thickness was reported in a time-domain terahertz study [24] of the system $(\text{Bi}_{1-x}\text{In}_x)_2\text{Se}_3$. Analysis of the real and imaginary parts of the Drude conductivity indicated a crossover thickness, $d_c(x)$, below which the carrier scattering rate, $1/\tau$ increased rapidly. The crossover was associated with entering a regime where $\Delta_t(d) > 1/\tau$, which is the condition for loss of topological protection against backscattering. For $x = 0$, d_c is ~ 6 QL, which is comparable to, but somewhat smaller than, the thicknesses at which the remnant Θ_K changes abruptly in our somewhat similar but magnetically-doped films. That the crossover to strong coupling between top and bottom surfaces, as heralded by Θ_K dropping to zero, occurs at a larger thickness in the magnetic film is consistent with the expected reduction spin-orbit coupling strength that results from Cr-doping [25, 26]. The smaller spin-orbit coupling reduces the inverted bulk band gap, consequently increasing the penetration depth into the bulk of Dirac surface states. In the earlier study, below d_c the terahertz conductance decreases smoothly but extrapolates to zero at $d \approx 2$ QL. The absence of conductance at 2 QL was associated with either the theoretically expected transition to a topologically trivial state, or strong disorder in the ultrathin limit. As shown in Fig. 2, $\Theta_K(\omega)$ shows an analogous transition to zero response at this same thickness.

The pronounced structure that we observe in $\Theta_K(d)$ likely reflects a strong dependence of spin interactions on film thickness. This dependence, in turn, is a consequence of the complicated spin interactions that exist even in the thick film regime. Theoretical studies [27–29] have found that the effective interaction between impurity spins, as mediated by TI surface state electrons, is highly anisotropic because of the spin-momentum locking of the DBs. The interaction is characterized by an Ising term, $U_{12} = -J_z S_1^z S_2^z$, that favors FM alignment in the direction normal to the film plane as is experimentally observed in our thicker films, plus contributions that depend on the relative position, \mathbf{r} , of the spins. One such contribution favors FM alignment in the direction parallel to \mathbf{r} and the other favors anti-FM (AFM) alignment in the direction perpendicular to \mathbf{r} . If the position-dependent terms are sufficiently weak, the ground state has FM order along z . However, if the position-dependent interactions are strong enough the ground state will be a spin glass [29].

Two recent theoretical studies have considered the dependence of these competing interactions on film thickness [30, 31]. As pointed out in Ref. [31], the Ising FM interaction arises mainly from excitations across the gap, and therefore decreases monotonically with d due to in-

creased $\Delta_t(d)$. On the other hand, the AFM interactions, which derive from superexchange, depend only weakly on the gap, and consequently on thickness. Therefore, as films become sufficiently thin, the AFM interaction will eventually dominate, in which case the random distribution of magnetic impurities [32] will frustrate an AFM ground state and lead to paramagnetic or spin glass behavior.

A similar conclusion was reached in Ref. [30], in which the dependence of the effective interaction on the distance of the impurities from the surface was included. In that work it was reported that, while the Ising interaction mediated by a single surface state is FM, in agreement with previous work [27–29], the interaction between spins situated near opposite surfaces is AFM. For a film that is sufficiently thin, interactions that favor alignment along z can be frustrated by positional disorder and the net weakening of the Ising contribution to the exchange energy can again lead to spin glass behavior. Our observation that as opposite surfaces approach each other the remnant magnetization vanishes, while the film retains a large susceptibility to external fields, is consistent with both the above theoretical pictures.

In summary, we have measured the complex magneto-optic Kerr effect in $(\text{Cr}_{0.12}\text{Bi}_{0.26}\text{Sb}_{0.62})_2\text{Te}_3$ in visible and near-IR wavelengths as a function of temperature, photon energy and magnetic field. We observed a resonant enhancement of the Kerr effect at 1.7 eV corresponding to the energy of a second Dirac node relative to the chemical potential. The enhanced Kerr effect allowed us to explore the effective time-reversal breaking field Δ_z in the ultrathin film limit. At our base temperature of 6 K, we observe a transition to zero remnant magnetization below a thickness of 8 QL, and to essentially zero magnetism at 2 QL. The variation of Δ_z is consistent with theories of thickness dependence of magnetic impurity spin interaction in TIs.

Research primarily supported by the U.S. Department of Energy, Office of Science, Basic Energy Sciences, under Contract No. DE-AC02-76SF00515. J. G. acknowledges a scholarship from the Materials Science and Active Surface Program at Ecole Polytechnique, Palaiseau, France (Chaire X-ESPCI-Saint-Gobain) for support. K. L. W. acknowledges the support of the Raytheon endorsement. A. J. B. acknowledges support from a Benchmark Stanford Graduate Fellowship. E. J. F. acknowledges support from a DOE Office of Science Graduate Fellowship. Materials growth, surface characterization, preliminary electrical characterization, and electronic instrumentation were supported by the DARPA MESO program under Contracts No. N66001-12-1-4034 and No. N66001-11-1-4105. Infrastructure and cryostat were funded in part by the Gordon and Betty Moore Foundation through Grant GBMF3429 to D. G.-G.

* jworenstein@lbl.gov

- [1] X.-L. Qi and S.-C. Zhang, *Rev. Mod. Phys.* **83**, 1057 (2011).
- [2] M. Z. Hasan and C. L. Kane, *Rev. Mod. Phys.* **82**, 3045 (2010).
- [3] X.-L. Qi, T. L. Hughes, and S.-C. Zhang, *Phys. Rev. B* **78**, 195424 (2008).
- [4] A. M. Essin, J. E. Moore, and D. Vanderbilt, *Phys. Rev. Lett.* **102**, 146805 (2009).
- [5] L. He, X. Kou, and K. L. Wang, *Phys. Status Solidi RRL* **7**, 50 (2013).
- [6] Y. Zhang, K. He, C.-Z. Chang, C.-L. Song, L.-L. Wang, X. Chen, J.-F. Jia, Z. Fang, X. Dai, W.-Y. Shan, *et al.*, *Nature Phys.* **6**, 584 (2010).
- [7] R. Yu, W. Zhang, H.-J. Zhang, S.-C. Zhang, X. Dai, and Z. Fang, *Science* **329**, 61 (2010).
- [8] C.-Z. Chang, J. Zhang, X. Feng, J. Shen, Z. Zhang, M. Guo, K. Li, Y. Ou, P. Wei, L.-L. Wang, *et al.*, *Science* **340**, 167 (2013).
- [9] X. Kou, S.-T. Guo, Y. Fan, L. Pan, M. Lang, Y. Jiang, Q. Shao, T. Nie, K. Murata, J. Tang, *et al.*, *Phys. Rev. Lett.* **113**, 137201 (2014).
- [10] J. Bestwick, A., J. Fox, E., X. Kou, L. Pan, K. L. Wang, and D. Goldhaber-Gordon, *Phys. Rev. Lett.* **114**, 187201 (2015).
- [11] M. Lasia and L. Brey, *Phys. Rev. B* **90**, 075417 (2014).
- [12] W.-K. Tse and A. H. MacDonald, *Phys. Rev. B* **84**, 205327 (2011).
- [13] W.-K. Tse and A. H. MacDonald, *Phys. Rev. Lett.* **105**, 057401 (2010).
- [14] X. Wang, J. Lian, Y. Huang, Z. Sun, J. Liu, F. Zhang, S. Gao, X. Yu, P. Li, and M. Zhao, *Jpn. J. Appl. Phys.* **52**, 103001 (2013).
- [15] K. Sato, *Jpn. J. Appl. Phys.* **20**, 2403 (1981).
- [16] J. Badoz, M. Billardon, J. Canit, and M. Russel, *J. Opt.* **8**, 373 (1977).
- [17] See Supplemental Material for (i) a more complete description of the Kerr analysis and results, and (ii) transport characterization of magnetic TI films used in this study.
- [18] J. A. Sobota, S.-L. Yang, A. F. Kemper, J. Lee, F. T. Schmitt, W. Li, R. G. Moore, J. G. Analytis, I. R. Fisher, P. S. Kirchmann, *et al.*, *Phys. Rev. Lett.* **111**, 136802 (2013).
- [19] D. Niesner, T. Fauster, S. Eremeev, T. Menshchikova, Y. M. Koroteev, A. Protogenov, E. V. Chulkov, O. Tereshchenko, K. Kokh, O. Alekperov, *et al.*, *Phys. Rev. B* **86**, 205403 (2012).
- [20] S. Eremeev, I. Silkin, T. Menshchikova, A. P. Protogenov, and E. V. Chulkov, *JETP Lett.* **96**, 780 (2013).
- [21] J.-W. Park, S. H. Baek, T. D. Kang, H. Lee, Y.-S. Kang, T.-Y. Lee, D.-S. Suh, K. J. Kim, C. K. Kim, Y. H. Khang, *et al.*, *Appl. Phys. Lett.* **93**, 021914 (2008).
- [22] E. Kojima, R. Shimano, Y. Hashimoto, S. Katsumoto, Y. Iye, and M. Kuwata-Gonokami, *Phys. Rev. B* **68**, 193203 (2003).
- [23] C. Sun, J. Kono, Y.-H. Cho, A. K. Wójcik, A. Belyanin, and H. Munekata, *Phys. Rev. B* **83**, 125206 (2011).
- [24] L. Wu, M. Brahlek, R. V. Aguilar, A. Stier, C. Morris, Y. Lubashevsky, L. Bilbro, N. Bansal, S. Oh, and N. Armitage, *Nature Phys.* **9**, 410 (2013).
- [25] J. Zhang, C.-Z. Chang, P. Tang, Z. Zhang, X. Feng, K. Li, L.-L. Wang, *et al.*, *Science* **339**, 1582 (2013).
- [26] X. Kou, L. Pan, J. Wang, Y. Fan, E. S. Choi, W.-L. Lee, T. Nie, K. Murata, Q. Shao, S.-C. Zhang, *et al.*, arXiv preprint arXiv:1503.04150 (2015).
- [27] Q. Liu, C.-X. Liu, C. Xu, X.-L. Qi, and S.-C. Zhang, *Phys. Rev. Lett.* **102**, 156603 (2009).
- [28] J.-J. Zhu, D.-X. Yao, S.-C. Zhang, and K. Chang, *Phys. Rev. Lett.* **106**, 097201 (2011).
- [29] D. A. Abanin and D. A. Pesin, *Phys. Rev. Lett.* **106**, 136802 (2011).
- [30] V. I. Litvinov, *Phys. Rev. B* **89**, 235316 (2014).
- [31] J. Wang, B. Lian, and S.-C. Zhang, arXiv preprint arXiv:1412.8237 (2014).
- [32] I. Lee, C. K. Kim, J. Lee, S. J. L. Billinge, R. Zhong, J. A. Schneeloch, T. Liu, T. Valla, J. M. Tranquada, G. Gu, and J. C. S. Davis, *Proc. Natl. Acad. Sci.* **112**, 1316 (2015).

SUPPLEMENTARY INFORMATION

SPECTROSCOPY DATA ACQUISITION

We use a technique based on a photo-elastic optical phase modulator [15, 16] to measure the real and imaginary parts of the Kerr effect. By itself, this technique does not discriminate time-reversal breaking from birefringence as a source of Kerr rotation. Thus, there are several possible contributions to the experimentally measured signal, in addition to the magneto-optic Kerr rotation of the sample: possible birefringence of the sample and cryostat window, and (in the presence of an applied field) the Faraday effect of the window.

To isolate the magneto-optic Kerr effect of the sample, we use the following procedure, which is illustrated in Fig. S1. We first measure the spectrum of Θ_K , in both positive and negative magnetic fields at $T \approx 50$ K where the samples are known to nonmagnetic, as shown in Fig. S1a. We then measure Θ_K with the sample cooled to the desired temperature, for example 6 K as in Fig. S1, again for both positive and negative magnetic fields. We then calculate the difference spectra, $\Theta_K(6K, +B) - \Theta_K(50K, +B)$ and $\Theta_K(6K, -B) - \Theta_K(50K, -B)$, shown in Fig. S1b. Since the sample is cooled independently of its environment, this eliminates the Faraday and birefringence effects coming from the cryostat windows (which are always at room temperature). Finally, we calculate the component of the spectra in Fig. S1b that is anti-symmetric in applied magnetic field to obtain the time-reversal symmetry breaking magneto-optic Kerr effect.

Magnetic field dependence

As noted in the main text, for samples with thickness $d \geq 10$ QL, significant magnetization appears with very small applied fields in the T range 20 – 50 K, where the

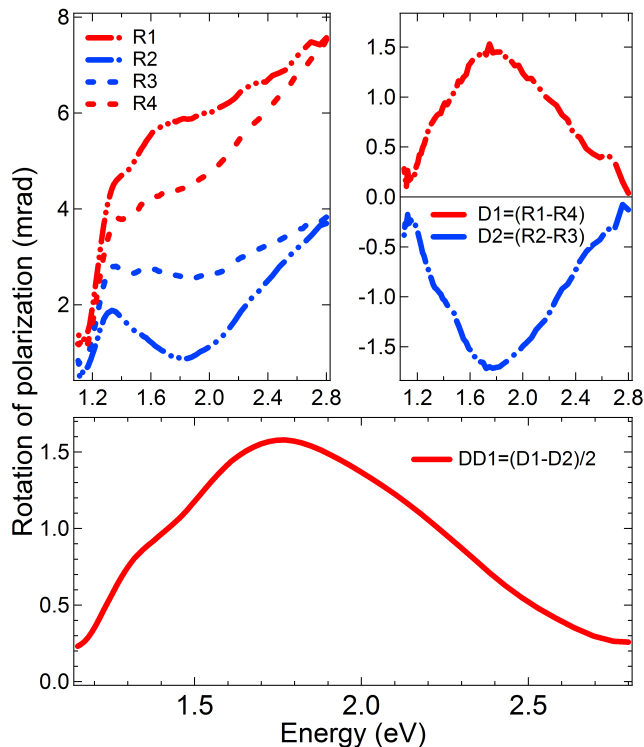


FIG. 4. Isolating the magneto-optic Kerr effect at 6 K for 20 QL sample. (a) Θ_K at 6 K in +100 mT (R1), and -100mT (R2), and at 50 K in field -100mT (R3) and +100mT (R4). (b) Θ_K at 50 K subtracted from Θ_K at 6 K in field +100mT (D1) and -100mT (D2). (c) Field antisymmetric component of the data (DD1).

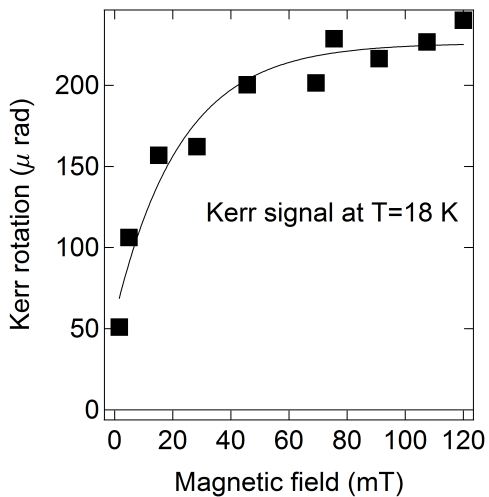


FIG. 5. Magnetic field dependence of Kerr signal at 18 K in a sample with $T_r=10$ K at photon frequency of 1.96 eV. The thin solid line is a guide to the eye.

remnant magnetization is unmeasurably small. As an illustration of this effect, in Fig. S2 we plot Θ_K vs. field at $T=18$ K for a sample in which the remnant magnetization signal vanishes above 10 K. A nonzero Θ_K is measurable to fields as small as 2 mT.

TRANSPORT CHARACTERIZATION

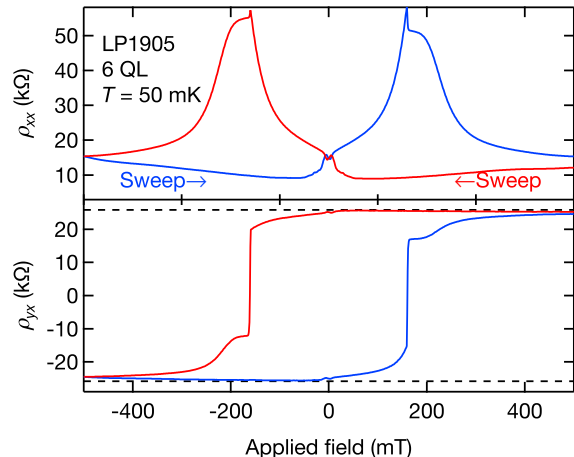


FIG. 6. Sample hysteresis loop of magnetic TI film measured in transport, showing longitudinal resistivity ρ_{xx} (top panel) and anomalous Hall resistivity ρ_{yx} (bottom panel) as a function of applied magnetic field. In this case the sample resistances approached the quantized values associated with the QAHE.

In addition to making magneto-optic Kerr effect measurements, we also characterized magnetic TI films by transport at a range of temperatures. After their growth via molecular-beam epitaxy, the GaAs (111) wafers were cleaved into several smaller pieces, allowing for the same films be measured in both electronic and magneto-optic apparatuses. To form transport devices, films were manually scratched into Hall bar shapes using a sharp metal tip, and indium was placed on each terminal to form Ohmic contacts [8, 10]. Devices sizes were typically 2×1 mm. The longitudinal and Hall resistivities were measured using standard lock-in techniques in a dilution refrigerator with base temperature ~ 40 mK.

All devices demonstrated robust ferromagnetism at cryogenic temperatures, as measured by the anomalous Hall effect. An example hysteresis loop is shown in Fig. 2, in which the out-of-plane magnetization, reflected by the anomalous Hall resistivity ρ_{yx} , of the sample can be switched between up and down by applying magnetic fields larger than the coercivity. Upon heating the sample to 40 K, above the Curie temperature, the conventional Hall effect was used to extract sample carrier concentrations. Table I contains the complete list

Growth name	Thickness	Al ₂ O ₃ cap?	In Fig.	Hall density at 40 K (10 ¹² cm ⁻²)	Peak ρ_{yx} at 50 mK (k Ω)
LP2278	2 QL	no	2	–	–
LP2038	3 QL	no	3b	2.8	–
LP2277	3 QL	no	2	–	–
LP2275	4 QL	no	2	–	–
LP1906	5 QL	yes	–	-1.8	12.2
LP2039	5 QL	no	3b	-7.0	–
LP2271	5 QL	no	2	–	–
LP1905	6 QL	yes	–	-2.1	25.1
LP2276	6 QL	no	2	–	25.0
LP1904	7 QL	yes	–	-2.0	12.2
LP2040	7 QL	no	3b	9.1	17.1
LP2272	8 QL	no	2	–	25.8
LP2041	9 QL	no	3b	-7.9	5.0
LP1989	10 QL	yes	3b	-4.1	2.6
LP2274	10 QL	no	2	–	–
LP1990	15 QL	yes	3b	-2.8	7.2
LP1991	20 QL	yes	1, 3	-1.1	4.0

TABLE I. Transport characterizations of films used in this study. Listed for each films is the thickness, the presence or absence of an alumina capping layer, other figures in this paper where we report optical measurements of this film, the Hall density measured at 40 K, and the highest observed anomalous Hall resistance at base temperature. Note that for LP2038 and LP2039 the samples became insulating below 1 K, preventing anomalous Hall effect measurements. Hall densities at 40 K were not measured for LP2272 and LP2276. LP2278, LP2277, LP2275, LP2271, and LP2274 were not characterized in transport.

of transport characterizations. Hall densities ranged between -8×10^{12} (hole doped) to 9×10^{12} cm⁻² (electron doped), though the range was narrower among samples whose growth process included an *in situ* deposition of an alumina cap. Regardless, the differing carrier densities may explain some of the variation in anomalous Hall resistivities, which ranged from a few k Ω to near the quantized value $h/e^2 \approx 25.8$ k Ω associated with the QAHE.